

Continuum random phase approximation approach to charged-current neutrino-nucleus scattering

N. Jachowicz,* K. Heyde, J. Ryckebusch, and S. Rombouts

Institute for Subatomic and Radiation Physics, Ghent University, Proeftuinstraat, 86 B-9000 Gent, Belgium

(Received 17 July 2001; published 16 January 2002)

We present continuum random phase approximation (CRPA) calculations for charged-current neutrino-nucleus scattering. The CRPA formalism is based on a Green's-function approach, and the calculations can be done in a self-consistent fashion when using an effective nucleon-nucleon force of the Skyrme type. We analyze the technical aspects related to the description of charge-exchange reactions within this approach, and study the sensitivity of the results to the single-particle characteristics of the formalism. Muon capture is studied as a test case. In applications of the formalism, we concentrate on neutrino-scattering off ^{12}C and ^{16}O , and pay attention to interactions of experimental interest.

DOI: 10.1103/PhysRevC.65.025501

PACS number(s): 13.15.+g, 25.30.-c, 24.10.-i

I. INTRODUCTION

During the last decades, neutrinos and their interactions with nuclei have been attracting a great deal of attention. It has become obvious that neutrinos play a prominent role in various astrophysical processes, especially in the dynamics of core-collapse supernovae and supernova-nucleosynthesis, with the detection of neutrinos from SN1987A as an outstanding example. Moreover, neutrinos proved to be interesting tools for testing weak interaction properties, examining nuclear structure, and for exploring the limits of the standard model.

Whereas neutral-current neutrino scattering is important in astrophysical processes, experimental efforts mostly concentrate on charged-current reactions, mainly because of the fact that the outgoing charged leptons are more easily detected. Theoretically, however, charged-current reactions represent a more challenging problem as the transition to the final nucleus is not straightforwardly described by most formalisms. Several authors tackled these problems, using various approaches ranging from a relativistic Fermi-gas approach to the random-phase-approximation (RPA) and shell-model approaches [1–8].

In spite of these theoretical and experimental efforts, longstanding problems concerning the discrepancy between theoretical and experimental results for the reaction $^{12}\text{C}(\nu_\mu, \mu^-)^{12}\text{N}^*$ could not be solved satisfactorily [6–11]. These problems motivated a new study of charged-current neutrino-nucleus reactions, including a calculation of cross sections for nuclei of experimental interest.

The paper is organized as follows. Section II sketches the theoretical framework for determining the weak neutrino-nucleus cross sections. In Sec. III we present the main characteristics of the Hartree-Fock continuum random-phase-approximation (CRPA) formalism. Section IV highlights the adaptations which are necessary to deal with charge-exchange reactions within such a framework, and discusses the theoretical uncertainties which these adaptations bring

along. Muon capture rates are studied in Sec. V. Section VI presents results of our cross-section calculations, with applications for neutrino-scattering on ^{12}C and ^{16}O . We examine the sensitivity of the cross section to single-particle wave functions and to choices of the residual interaction. The validity of isospin symmetry in the description of these reactions is discussed.

II. CHARGE-EXCHANGE NEUTRINO-NUCLEUS SCATTERING

We consider semileptonic weak interactions in which a neutrino is scattered quasielastically from a nucleus. The initial nucleus is assumed to be spherically symmetric, and to reside in its ground state with angular momentum and parity $J^\pi=0^+$. In charged-current reactions, the outgoing particle is a massive lepton and the final nucleus will differ from the initial one by one charge unit. The nucleus is left in an excited state with final parity and angular momentum $J_f^{\pi_f}$. Denoting

$$\tilde{k}_f = \sqrt{1 - \frac{m_f^2}{\varepsilon_f^2}}, \quad (1)$$

the cross-section formula reads

$$\left(\frac{d^2\sigma_{i \rightarrow f}}{d\Omega d\omega} \right)_{\tilde{\nu}} = \frac{G^2 \cos^2 \theta_C \varepsilon_f^2}{\pi} \tilde{k}_f F(Z', E) \left[\sum_{J=0}^{\infty} \sigma_{CL}^J + \sum_{J=1}^{\infty} \sigma_T^J \right], \quad (2)$$

with

$$\begin{aligned} \sigma_{CL}^J &= \mathcal{F}^M |\langle J_f | \hat{\mathcal{M}}_J(\kappa) | J_i \rangle|^2 + \mathcal{F}^L |\langle J_f | \hat{\mathcal{L}}_J(\kappa) | J_i \rangle|^2 \\ &+ 2\mathcal{F}^{ML} \text{Re}[\langle J_f | \hat{\mathcal{L}}_J(\kappa) | J_i \rangle \langle J_f | \hat{\mathcal{M}}_J(\kappa) | J_i \rangle^*], \end{aligned} \quad (3)$$

$$\mathcal{F}^M = [1 + \tilde{k}_f \cos \theta], \quad (4)$$

*Present address: Institut für Physik der Universität Basel, Klingelbergstrasse 82, CH-4056 Basel, Switzerland. Email address: natalie.jachowicz@rug.ac.be.

$$\mathcal{F}^{\mathcal{L}} = \left[1 + \tilde{k}_f \cos \theta - \frac{2\varepsilon_i \varepsilon_f \tilde{k}_f^2 \sin^2 \theta}{\kappa^2} \right], \quad (5)$$

$$\mathcal{F}^{\mathcal{ML}} = \left[\frac{\omega}{\kappa} (1 + \tilde{k}_f \cos \theta) + \frac{m_f^2}{\varepsilon_f \kappa} \right] \quad (6)$$

and

$$\begin{aligned} \sigma_{\mathcal{F}}^J = & \mathcal{F}^{\mathcal{J}} [|J_f| |\hat{\mathcal{J}}_J^{mag}(\kappa)| |J_i|^2 + |J_f| |\hat{\mathcal{J}}_J^{el}(\kappa)| |J_i|^2] \\ & \mp 2 \mathcal{F}^{\mathcal{JJ}} \text{Re} [\langle J_f | \hat{\mathcal{J}}_J^{mag}(\kappa) | J_i \rangle \langle J_f | \hat{\mathcal{J}}_J^{el}(\kappa) | J_i \rangle^*], \end{aligned} \quad (7)$$

$$\mathcal{F}^{\mathcal{J}} = \left[1 - \tilde{k}_f \cos \theta + \frac{\varepsilon_i \varepsilon_f \tilde{k}_f^2 \sin^2 \theta}{\kappa^2} \right], \quad (8)$$

$$\mathcal{F}^{\mathcal{JJ}} = \left[\frac{\varepsilon_i + \varepsilon_f}{\kappa} (1 - \tilde{k}_f \cos \theta) - \frac{m_f^2}{\varepsilon_f \kappa} \right], \quad (9)$$

the Coulomb longitudinal [Eq. (3)] and transverse [Eq. (7)] response to the external field, respectively. The energy of the incoming and outgoing leptons are denoted by ε_i and ε_f respectively, m_f is the mass of the outgoing charged lepton, θ is the lepton scattering angle, and κ is the transferred momentum. The weak interaction coupling constant G was multiplied by the factor $\cos \theta_C$ in order to take into account Cabibbo mixing. The functions $\mathcal{M}_J(\kappa)$, $\mathcal{L}_J(\kappa)$, $\mathcal{J}_J^{el}(\kappa)$, and $\mathcal{J}_J^{mag}(\kappa)$ denote the Coulomb, longitudinal, transverse electric, and transverse magnetic multipole operators as defined in Ref. [12], where a nonrelativistic reduction of the hadron current is adopted. The momentum dependence of the form-factors is given by a dipole parametrization [13].

Charged-current neutrino scattering reactions always involve a charged particle in the exit channel. In principle its wave function should be obtained by solving the scattering equation of the ejected lepton in the Coulomb potential generated by the final nucleus. In this case the cross-section calculation would involve an extra integral over the momentum transfer. This folding procedure is often performed in an effective way by introducing the Fermi function $F(Z', E)$ [14]. The cross section is then multiplied by the square of the ratio between the correct scattering solution and a plane wave for a point charge Z' [15].

III. CONTINUUM RANDOM PHASE APPROXIMATION APPROACH

The transition densities required to determine the cross section [Eq. (2)] are obtained within a CRPA, which was described in great detail in Refs. [16–19]. The formalism is based on Green's-function techniques where the polarization propagator is obtained through iterating all possible particle-hole (ph) and hole-particle (hp) excitations of the ground state to all orders. Higher-order configurations of the $2p$ - $2h$, $3p$ - $3h$, \dots type are neglected.

The transition densities ρ^{RPA} are subsequently obtained as

the solutions of the CRPA version of the Lippmann-Schwinger equation

$$\rho^{RPA} = \frac{1}{1 - \mathcal{R}\mathcal{V}} \rho^0, \quad (10)$$

where \mathcal{R} and ρ^0 denote the unperturbed response function and transition densities, and \mathcal{V} describes the residual interaction. Within this formalism, hole-state wave functions and scattering solutions are obtained consistently from the same Schrödinger equation. The Green's-function formalism, moreover, allows one to treat the single-particle continuum in an exact way, thereby avoiding the commonly adopted approximations of discretizing the continuum and introducing an energy cutoff in the single-particle spectrum.

As residual interaction \mathcal{V} the SkE2-force [17,20–22] is used. This extended Skyrme parametrization was designed to yield a realistic description of nuclear structure in particle-particle as well as particle-hole channels, providing a strong tool in the description of both ground state and excited state nuclear properties over the whole mass table [21]. The SkE2-Skyrme interaction allows one to introduce the same force as residual interaction in Eq. (10) and in the Hartree-Fock calculation of the unperturbed single-particle quantities, which makes the calculations self-consistent with respect to the nucleon-nucleon force used. The formalism has proven its strength in the description of various electromagnetically induced nucleon knockout processes [16,17], and in cross-section calculations for neutral-current weak interactions [12].

IV. CHARGED-CURRENT TRANSITION DENSITIES

Whereas neutral-current reactions imply excitations within the same nucleus, charged-current neutrino scattering induces transitions to a daughter nucleus with a charge difference of one unit. The CRPA transition densities depend on single-particle energies and wave functions designed for a description of the target nucleus. As a consequence, the approach cannot be straightforwardly applied to a calculation of cross sections for charge-exchange reactions. The single-particle levels in the daughter nucleus correspond to different energies and should be dealt with using adapted radial wave functions. This is not easily done within the Green's-function formalism, making this CRPA approach as such not particularly suited to dealing with a description of the rearrangement effects related to the transition between different neighboring nuclei.

Instead of a cumbersome adaptation of the formalism to the single-particle structure in the final nucleus, charged-current matrix elements can be calculated within the initial nucleus, relying on the isospin symmetry between mother and daughter systems. A charged-current calculation can then be effectively made by computing the neutral-current transition densities to the isobaric analog state in the initial nucleus. Imposing isospin symmetry and applying the Wigner-Eckart theorem, the charged-current transition matrix element can be obtained from the isovector neutral-current ones,

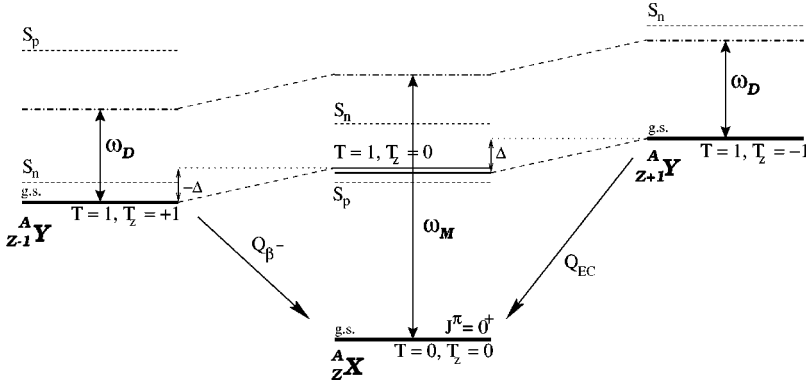


FIG. 1. Schematic representation of the energy balance parameters for transitions between states in different members of an isospin triplet.

$$\left\langle T=1, M_T = \pm 1 \left| \sum_{i=1}^A \tau_{\pm}^i \right| T=0, M_T = 0 \right\rangle = \frac{1}{\sqrt{2}} \left\langle T=1, M_T = 0 \left| \sum_{i=1}^A \tau_3^i \right| T=0, M_T = 0 \right\rangle, \quad (11)$$

where the matrix element on the right-hand side of this equation can be calculated using both initial and final states in the mother nucleus. In practice, one has to ascertain that the isospin projection is accurately performed, and only transitions to $T=1$ states in the initial system are considered in the calculation.

However tempting and theoretically elegant this solution may be, one has to be aware of the fact that Coulomb and charge-dependent terms in the nuclear forces partially break the isospin symmetry between initial and daughter nuclei. This is illustrated by the differences between the Q value for a reaction and the energy of the isobaric analog state in the initial nucleus of the daughter nuclear ground state (see Fig. 1).

It is clear that cross sections resulting from this approach may suffer from inaccuracies related to the assumptions made. Therefore, efforts were made to remain as close as possible to the experimental situation while exploiting the isospin symmetry. The transition densities are written as the product of lepton and hadron transitions:

$$\langle \Psi_f | \hat{O} | \Psi_i \rangle = \langle f_l | \hat{O}_l | i_l \rangle \langle f_h | \hat{O}_h | i_h \rangle. \quad (12)$$

With ω_M the excitation energy in the mother nucleus used in the hadron part of Eq. (12), Fig. 1 shows that the excitation energy in the daughter nucleus is given by

$$\omega_D = \omega_M - (Q - \Delta). \quad (13)$$

The energy of the outgoing lepton in Eq. (12) is then obtained as

$$\varepsilon_f = \varepsilon_i - Q - \omega_D \quad (14)$$

or

$$\varepsilon_f = \varepsilon_i - \omega_M - \Delta \quad (15)$$

for a transition to the isobaric analog state in the daughter nucleus of the state corresponding to an excitation energy ω_M in the initial system. Whereas the Q value arises from the fact that not all the energy available for the reaction can be used for the excitation of the daughter nucleus, the term Δ takes into account the fact that the Q value of the reaction does not coincide with the energy difference between the ground state of the mother nucleus and its isobaric analog state in the final nucleus (see Fig. 1). Although this approach is not completely consistent due to this energy difference Δ , it ascertains that the lepton kinematics are treated using the experimental Q value, while the calculation of the hadronic transition density exploits the isospin symmetry between initial and final systems. This is important as the dependence of the cross-section formula [Eq. (2)] on the square of the outgoing lepton energy ε_f^2 introduces a major sensitivity of the results to the lepton kinematics.

Apart from the kinematical caveats discussed in the previous paragraph, Fig. 1 illustrates some other aspects which ought to be carefully considered. In some cases it appears necessary to introduce a low-energy cut in the calculated CRPA strength distributions. Indeed, excitations to continuum states of the initial system may not have a corresponding transition in the daughter nucleus. When the continuum in the mother system opens at an energy smaller than $Q - \Delta$, this lower part of the spectrum has to be eliminated from the energy integral when comparing calculations with data. This is the case for the total ^{16}O cross sections calculated in this work. Moreover, due to the different values for the single-particle thresholds in mother and daughter nuclei, situations occur in which transitions to a discrete state are to be treated as transitions to a continuum state within the context of the CRPA framework. Uncertainties introduced by these approximations might then result in a limitation of the accuracy for the calculated cross sections.

The ambiguity in the energy-level structure, introduced by adopting the isospin approach based on the Wigner-Eckart theorem, has some further implications. The fact that all transition densities are determined within the initial nucleus implies that it has to be carefully examined which transitions are included in the CRPA cross section. In principle, only transitions to states in the daughter nucleus, for which the transition to the isobaric analog state in the initial nucleus is included in the CRPA cross section, are taken into account. However, this does not always agree with the picture one

TABLE I. Comparison between experimental muon capture rates (in units of 10^3 s^{-1}) and CRPA results for the reactions $^{16}\text{O}(\mu^-, \nu_\mu)^{16}\text{N}^*$ and $^{12}\text{C}(\mu^-, \nu_\mu)^{12}\text{B}^*$. In the CRPA calculation, Hartree-Fock single-particle wave functions were used, and the residual interaction is SkE2. The incoming muon wave function is treated as in Ref. [14]. All multipoles up to $J=5$ are taken into account. The experimental values of the single-particle thresholds were introduced in the calculation. The experimental capture rate for ^{12}C was corrected for the contribution of transitions to bound states in ^{12}B .

	Experiment [15]	CRPA
^{16}O	98	96.65
^{12}C	29.99	34.20

obtains from energy considerations based on the Q values for these reactions. As a consequence, the calculated ^{12}C cross sections will only include transitions to excited states.

V. MUON CAPTURE RATES

Muon capture rates are experimentally well established, and provide an important test for charged-current neutrino scattering calculations. Muon capture

$$X(Z,A) + \mu^- \rightarrow X(Z-1,A) + \nu_\mu \quad (16)$$

can be considered as the inverse of the charged-current neutrino reaction

$$X(Z,A) + \nu \rightarrow X(Z+1,A) + l^-. \quad (17)$$

With the incoming muon wave function treated as in Ref. [14], the transition densities entering the cross-section formula are the same in both reactions; thus muon capture rates provide stringent tests of the computed neutrino scattering cross sections. Moreover the momentum transfer in muon capture ($m_\mu \sim 105.7 \text{ MeV}$) coincides rather well with the energy region considered here.

Table I summarizes the rates for muon capture on ^{12}C and ^{16}O resulting from the present calculations, and compares them with the experimental values. The excellent agreement between the CRPA results and the experimental muon capture rates illustrates the reliability of the presented self-

TABLE II. Dominating multipole contributions to the reaction $^{12}\text{C}(\nu_\mu, \mu^-)^{12}\text{N}^*$. In the HFSk calculation, Hartree-Fock single-particle wave functions were used with the SkE2 Skyrme parametrization as residual interaction. In the WSSk results, single-particle wave functions were obtained from a Woods-Saxon potential.

	$J^\pi=1^-$	$J^\pi=1^+$	$J^\pi=2^-$	$J^\pi=2^+$	$J^\pi=3^-$	$J^\pi=3^+$
HFSk	25.3%	9.60%	18.7%	12.4%	8.34%	8.96%
WSSk	25.5%	10.8%	10.1%	17.7%	9.77%	11.6%

consistent calculations in cross-section calculations for charged-current neutrino scattering reactions.

VI. RESULTS AND DISCUSSION

In Fig. 2, we carry out a comparison between charged and neutral-current cross sections for neutrino scattering on ^{12}C . The figure clearly illustrates that charge-exchange cross sections are enhanced compared to neutral-current ones. This is mainly due to the isospin suppression of neutral-current transitions. Furthermore, the reaction $^{12}\text{C}(\nu_e, e^-)^{12}\text{N}^*$ has a considerably larger cross section than the antineutrino scattering reactions $^{12}\text{C}(\bar{\nu}_e, e^+)^{12}\text{B}^*$. Next to the influence of the sign difference of the transverse interference contribution to the cross-section formula [Eq. (2)] for neutrino and antineutrino scattering, this difference can also be attributed to the Coulomb interaction between the residual nucleus and the outgoing lepton.

As experimentally the scattering reactions are performed using neutrinos originating from decay reactions, we folded the cross sections with appropriate neutrino energy distributions. For reactions with relatively low momentum transfer, neutrinos are obtained from pion decay at rest and the subsequent decay of the muon, providing electron neutrinos distributed according to the Michel spectrum [23], with energies up to 52.8 MeV. For scattering reactions with muon neutrinos and antineutrinos as projectile particles, the energies in the Michel spectrum are not sufficient to make charged-current reactions feasible. These reactions are performed using neutrinos produced by pion decay in flight. This provides muon neutrinos and antineutrinos with energies up to approximately 300 MeV. The decay-in-flight spectra were normalized as

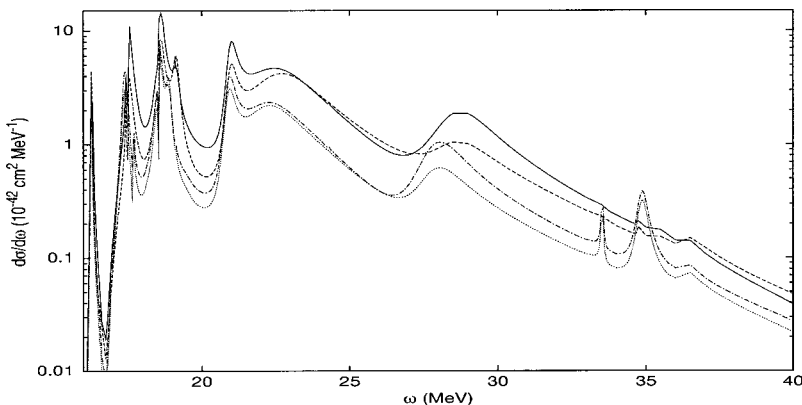


FIG. 2. Comparison between neutral and charged-current neutrino scattering on ^{12}C : $^{12}\text{C}(\nu, \nu')^{12}\text{C}^*$ (dash-dotted line), $^{12}\text{C}(\bar{\nu}, \bar{\nu}')^{12}\text{C}^*$ (dotted line), $^{12}\text{C}(\bar{\nu}_e, e^+)^{12}\text{B}^*$ (dashed line), and $^{12}\text{C}(\nu_e, e^-)^{12}\text{N}^*$ (full line). The incoming neutrino energy is 50 MeV. To facilitate the comparison between the different plots, for charged as well as for neutral-current reactions the ω values on the abscissa denote excitation energies in ^{12}C . For charge-exchange reactions, the values of the excitation energies in the daughter nucleus can easily be obtained by a shift of the excitation spectrum.

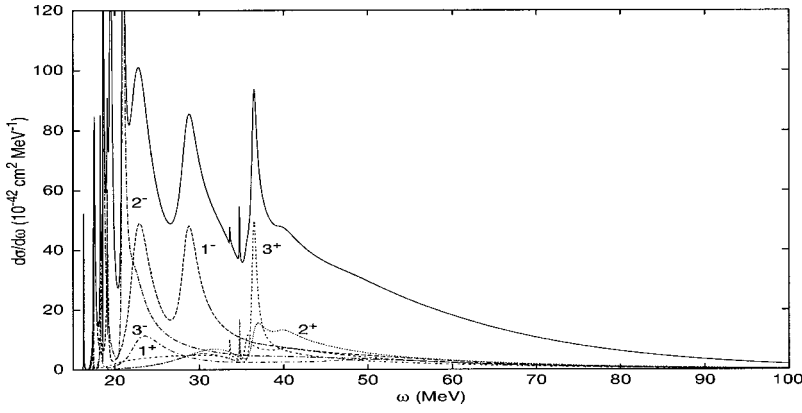


FIG. 3. Cross section for the reaction $^{12}\text{C}(\nu_\mu, \mu^-)^{12}\text{N}^*$ (full line) and dominant multipole contributions. The incoming neutrino spectrum is that from pion decay in flight. The scale on the ω axis refers to excitation energies in the nucleus ^{12}C . The single-particle wave functions were obtained by a Hartree-Fock calculation. As residual interaction the SkE2 Skyrme parametrization was adopted. For the single-particle energies, experimental values were used.

$$n_\nu(\varepsilon_i) = \frac{f(\varepsilon_i)}{\int_{E_{\text{thres}}}^{\infty} f(\varepsilon) d\varepsilon}. \quad (18)$$

Figure 3 shows the differential $^{12}\text{C}(\nu_\mu, \mu^-)^{12}\text{N}^*$ cross section for scattering of pion decay-in-flight neutrinos and its dominating multipole contributions. The relatively high-momentum transfer in this reaction enhances higher-order multipole transitions, especially at excitation energies above 30 MeV. The relative contributions of the most important multipoles are listed in Table II, showing the dominance of the $J^\pi = 1^-, 2^-, 2^+$, and 3^+ transitions. Due to the absence of a transverse contribution to these transitions [Eq. (2)], $J = 0$ contributions are suppressed.

Figures 4 and 5 illustrate the angular dependence of the cross section for this reaction and for the equivalent antineutrino scattering cross section $^{12}\text{C}(\bar{\nu}_\mu, \mu^+)^{12}\text{B}^*$, showing the cross section as a function of the excitation energy of the nucleus and the scattering angle of the outgoing lepton. Unlike the situation in neutral-current scattering, where we found backscattering to be prominent, the charged-current muon neutrino scattering strengths is more evenly distributed over the scattering angle of the outgoing lepton. For most resonances, the major fraction of the strength is localized in the lepton angle range between 70° and 150° .

Table III summarizes the cross sections and compares them with the experimental result, when available. For the reaction $^{12}\text{C}(\nu_e, e^-)^{12}\text{N}^*$ our results are in equally good agreement with the experimental result as the muon capture rates. Moreover, for these reactions we obtain good agree-

ment with the calculations of other authors [3,6,25]. Our self-consistent calculations mainly differ from the latter ones by the way the CRPA equations are solved. In Refs. [3,6] the standard RPA equations were extended into the continuum by the introduction of an energy integral, and solved by an expansion in Weinberg states. Single-particle wave functions were obtained with a Woods-Saxon potential, and the residual interaction was either a Landau-Migdal force or an effective force derived from the Bonn potential. Furthermore Ref. [6] examined the influence of a partial $p_{1/2}$ occupation, which was shown to induce a small reduction of the transition strength. Table III compares these cross sections with our results.

The fact that the $^{12}\text{C}(\nu_\mu, \mu^-)^{12}\text{N}^*$ strength overshoots the data by a factor of 2, seems quite remarkable considering the fair agreement obtained for the muon capture rate and the $^{12}\text{C}(\nu_e, e^-)^{12}\text{N}^*$ cross section. It is worth stressing, however, that the ν_μ -induced reaction probes higher neutrino energies. The larger outgoing lepton mass makes other operators and reaction mechanisms important. Moreover, the opposite isospin direction of muon capture and charged-current neutrino-scattering reactions involves final states in a different nucleus. The observed discrepancy with the data can very likely be explained by the problems concerning the description of charged-current scattering reactions discussed in Sec. IV, combined with the influence of deformation correlations in ^{12}C . This is corroborated by recent large-basis shell-model calculations, pointing to the fact that the inclusion of higher-order configurations in the cross-section calculation may account for the discrepancy between theory and experiment [7,8].

$$d^2\sigma/d\omega d\theta (10^{-42} \text{ cm}^2 \text{ MeV}^{-1} \text{ deg}^{-1})$$

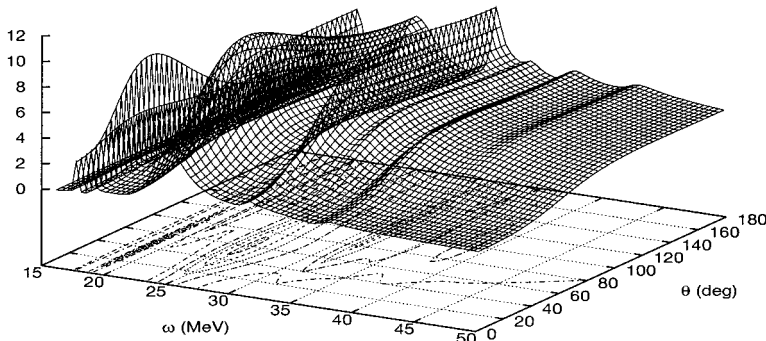


FIG. 4. Cross section for the charged-current reaction $^{12}\text{C}(\nu_\mu, \mu^-)^{12}\text{N}^*$ as a function of the excitation energy in ^{12}C and the lepton scattering angle θ . The incoming neutrino energy is distributed according to the pion decay-in-flight spectrum. The single-particle wave functions were obtained with a Woods-Saxon calculation. As residual interaction the SkE2 Skyrme parametrization was adopted. For the single-particle energies, experimental values were used.

TABLE III. CRPA cross sections for charged-current reactions on ^{12}C and ^{16}O . The ^{16}O cross sections are all inclusive, and for the ^{12}C reactions only transitions to excited states in the daughter nucleus are included. Cross sections are in units of 10^{-42} cm 2 , with exponents given between brackets. In the HFsk calculation Hartree-Fock single-particle wave functions were used, and the residual interaction is SkE2. The WSSk cross sections were obtained using Woods-Saxon single-particle parameters. The third line gives results for the Hartree-Fock SkE2 calculation, with single-particle energies averaged over the proton and neutron values as in Eqs. (19) and (20). When available, the theoretical values are compared with the experimental cross sections and the results of [6], obtained with a partial occupation of the $p_{1/2}$ subshell and the Bonn potential force.

	$^{12}\text{C}(\nu_e, e^-)^{12}\text{N}^*$	$^{12}\text{C}(\nu_\mu, \mu^-)^{12}\text{N}^*$	$^{12}\text{C}(\bar{\nu}_\mu, \mu^+)^{12}\text{B}^*$	$^{16}\text{O}(\nu_e, e^-)^{16}\text{N}$	$^{16}\text{O}(\nu_\mu, \mu^-)^{16}\text{F}$	$^{16}\text{O}(\bar{\nu}_\mu, \mu^+)^{16}\text{N}$
HFsk	6.19	23.7(2)	5.73(2)	9.43	30.4(2)	6.77(2)
WSSk	3.28	18.5(2)	3.98(2)	6.67	30.6(2)	6.68(2)
HFsk [Eqs. (19) and (20)]	4.78	22.5(2)	5.39(2)	7.64	29.7(2)	6.69(2)
Data	6.4 [9]; 5.7 [10]	10.5(2) [11]				
Ref. [6]	5.4	17.1(2)				

In order to gain more insight into the sensitivity of the $^{12}\text{C}(\nu_\mu, \mu^-)^{12}\text{N}^*$ cross section to the different model assumptions, we repeated the calculation with a Landau-Migdal force instead of the Skyrme interaction, and with single-particle wave functions obtained from a Woods-Saxon potential [24] instead of the Hartree-Fock calculation. While the choice of the residual interaction turned out to be of minor importance, the single-particle potential has a large impact on the final results. A CRPA calculation with Woods-Saxon single-particle wave functions for the $^{12}\text{C}(\nu_\mu, \mu^-)^{12}\text{N}^*$ reaction resulted in a total cross section of 18.5×10^{-40} cm 2 , in close agreement with the results obtained by Kolbe and co-workers [6,25]. The calculations we carried out using the Woods-Saxon potential, however, failed to reproduce an accurate value for the cross sections of the other reactions listed in Table III, and therefore seem less reliable than a self-consistent Hartree-Fock CRPA approach.

In practice, isospin projection remains a problem, especially in the region near the particle-emission threshold where there exists a basic asymmetry between protons and neutrons, introduced by the Coulomb interaction. One has to achieve a balance between an accurate description of the structure of the target nucleus, on the one hand, and imposing isospin symmetry on the other hand. Where the former implies the use of different single-particle energies and wave functions for protons and neutrons, the latter assumes an exact symmetry, between the proton and neutron single-particle properties. We therefore studied the effects arising when proton and neutron contributions are symmetrized and hence the

isospin symmetry is partially restored. Calculations were repeated with average values for the proton and neutron single-particle energies. This allows one to construct the wave functions

$$|ph^{-1}; T=0\rangle = \frac{1}{\sqrt{2}}\{|ph^{-1}\rangle_\pi + |ph^{-1}\rangle_\nu\}, \quad (19)$$

$$|ph^{-1}; T=1\rangle = \frac{1}{\sqrt{2}}\{|ph^{-1}\rangle_\pi - |ph^{-1}\rangle_\nu\}, \quad (20)$$

with definite isospin symmetry. As Table III shows, our analysis illustrates that due to the deviation from the experimental energy scheme introduced by this approach, results do not benefit from this alternative treatment of the isospin symmetry.

In summary, we studied charge-exchange neutrino-nucleus scattering reactions in a self-consistent fashion within a CRPA formalism based on a Green's-function approach. Special attention was paid to a description of the isospin complications that show up when carrying out charged-current CRPA calculations. For muon capture as well as neutrino scattering at low momentum transfer, our results are in excellent agreement with other theoretical calculations and with the experimental values. The cross sections obtained for the reaction $^{12}\text{C}(\nu_\mu, \mu^-)^{12}\text{N}^*$, however, showed obvious discrepancies when comparing with calculations from other authors as well as with the experimentally

$d^2\sigma/d\omega d\theta$ (10^{-42} cm 2 MeV $^{-1}$ deg $^{-1}$)

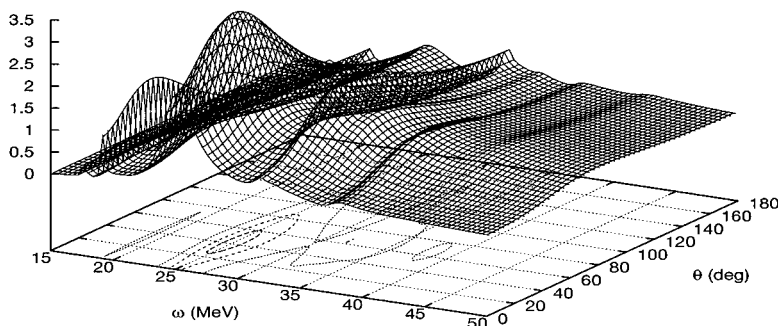


FIG. 5. Cross section for the charged-current reaction $^{12}\text{C}(\bar{\nu}_\mu, \mu^+)^{12}\text{B}^*$ as a function of the excitation energy in ^{12}C and the lepton scattering angle θ . The scale on the ω -axis refers to excitation energies in the nucleus ^{12}C . The incoming neutrino energies are distributed according to the pion decay-in-flight spectrum. The single-particle wave functions were obtained with a Woods-Saxon calculation. As residual interaction the SkE2 Skyrme parametrization was adopted. For the single-particle energies, experimental values were used.

obtained value. Whereas results using different residual interactions are in good agreement, the computed cross section proved to be sensitive to the single-particle input. These sensitivities are clear indications that more complex nuclear configurations should be incorporated in order to give a more stable description of both the excitation energies and widths of various resonances for the ^{12}C nucleus, known to be deformed in its ground state. However, the observed sensitivities mainly affected total cross-section rates, and proved to be irrelevant for many other aspects of the cross section. Our numerical calculations predict that the main multipole con-

tributions to the $^{12}\text{C}(\nu_\mu, \mu^-)^{12}\text{N}^*$ reaction are $J^\pi = 1^-, 2^-,$ and 3^+ , and that the strength is mainly concentrated at lepton scattering angles around 100° .

ACKNOWLEDGMENTS

The authors would like to thank K. Langanke, E. Kolbe, I. Borzov, and S. Goriely for interesting discussions. N.J. and S.R. are grateful to the Fund for Scientific Research (FWO) Flanders for financial support.

-
- [1] W. M. Alberico, M. B. Barbaro, S. M. Bilenky, J. A. Caballero, C. Giunti, C. Maieron, E. Moya de Guerra, and J. M. Udías, *Nucl. Phys.* **A623**, 471 (1997).
 - [2] H. Kim, J. Piekarewicz, and C. J. Horowitz, *Phys. Rev. C* **51**, 2739 (1995).
 - [3] E. Kolbe, K. Langanke, S. Krewald, and F. K. Thielemann, *Nucl. Phys.* **A540**, 599 (1992).
 - [4] S. K. Singh, N. C. Mukhopadhyay, and E. Oset, *Phys. Rev. C* **57**, 2687 (1998).
 - [5] J. Engel, E. Kolbe, K. Langanke, and P. Vogel, *Phys. Rev. C* **54**, 2740 (1996).
 - [6] E. Kolbe, K. Langanke, and P. Vogel, *Nucl. Phys.* **A652**, 91 (1999).
 - [7] A. C. Hayes and I. S. Towner, *Phys. Rev. C* **61**, 044603 (2000).
 - [8] C. Volpe, N. Auerbach, G. Colò, T. Suzuki, and N. Van Giai, *Phys. Rev. C* **62**, 015501 (2000).
 - [9] B. Zeitnitz, *Prog. Part. Nucl. Phys.* **32**, 351 (1994).
 - [10] R. Imlay, *Nucl. Phys.* **A629**, 531c (1998).
 - [11] C. Athanassopoulos *et al.*, *Phys. Rev. C* **56**, 2806 (1997).
 - [12] N. Jachowicz, S. Rombouts, K. Heyde, and J. Ryckebusch, *Phys. Rev. C* **59**, 3246 (1999).
 - [13] E. J. Beise and R. D. McKeown, *Comments Nucl. Part. Phys.* **20**, 105 (1991).
 - [14] J. D. Walecka, in *Muon Physics II—Weak Interactions*, edited by V. W. Hughes and C. S. Wu (Academic, New York, 1975).
 - [15] T. Suzuki, D. F. Measday, and J. P. Roalsvig, *Phys. Rev. C* **35**, 2212 (1987).
 - [16] J. Ryckebusch, M. Waroquier, K. Heyde, J. Moreau, and D. Ryckbosch, *Nucl. Phys.* **A476**, 273 (1988).
 - [17] J. Ryckebusch, K. Heyde, D. Van Neck, and M. Waroquier, *Nucl. Phys.* **A503**, 694 (1989).
 - [18] G. F. Bertsch and S. F. Tsai, *Phys. Rep.* **18C**, 125 (1975).
 - [19] S. F. Tsai, *Phys. Rev. C* **17**, 1862 (1978).
 - [20] M. Waroquier, J. Sau, K. Heyde, P. Van Isacker, and H. Vincx, *Phys. Rev. C* **19**, 1983 (1979).
 - [21] M. Waroquier, K. Heyde, and G. Wenes, *Nucl. Phys.* **A404**, 269 (1989).
 - [22] M. Waroquier, J. Ryckebusch, J. Moreau, K. Heyde, N. Blasi, S. Y. van de Werf, and G. Wenes, *Phys. Rep.* **148**, 249 (1987).
 - [23] C. Athanassopoulos *et al.*, *Nucl. Instrum. Methods Phys. Res. A* **388**, 149 (1997).
 - [24] G. Co' and S. Krewald, *Phys. Lett.* **137B**, 145 (1984).
 - [25] E. Kolbe (private communication).